Air Permeability and Thermal Performance of Concrete Block Wall Sections

Rachel Becker, PhD

ABSTRACT

Air permeability of 1.25 × 1.25 m block wall sections was measured in the 0–200 Pa range by means of a pressure box. Extrapolating results to a standard 100 m^2 dwelling indicated that nonrendered autoclaved-aerated-concrete block walls are extremely airtight, leading to an estimated leakage rate of 0.01–0.02 ach under 150 Pa; nonrendered regular-aggregate-concrete block walls, as well as lightweight-aggregate-concrete blocks, are highly permeable, with estimated rates of ~2–6 ach and ~5–10 ach under 50 and 150 Pa, respectively. An external 3 mm cementitious brown coat reduced these values to 0.07–0.16 ach and 0.18–0.21 ach. An internal 10 mm lime-cement rendering reduced them to 0.07–0.13 ach and 0.16–0.19 ach.

Thermal resistances of the hollow-core specimens were estimated by comparing temperature differences across specimens, measured by means of an insulated box, to estimated room-side surface resistances. A small pressure difference induced across specimens (0.1–1.0 Pa) decreased the estimated heat-flow rates but did not affect estimated R-values.

INTRODUCTION

Orme (2001) estimated the effect of infiltration rates in buildings on the energy consumption, CO_2 emissions, and monetary expenditure for 13 heating-dominated countries. Infiltration rates varied between 0.4 (Sweden) to 0.75 (Belgium) ach. Apparently, a third of the energy delivered for heating and cooling is attributed to air change losses, 30% to heat conduction losses, 27% to heating equipment losses, and 10% to delivered space cooling. He foresees that with the increasing demand for higher levels of thermal insulation, the relative contribution of infiltration will increase significantly. Similarly, Probst (2004) showed that under Monterey, California, weather conditions, infiltration may cause as much as a 50% increase in cooling energy consumption even when a relatively airtight building envelope (with a total rate of 0.5 ach) is applied. Dale et al. (Dale et al. 1985; Kostiuk and Dale 1987) measured the impact of various factors, including total natural infiltration, on the power consumption in two similar test rooms. They observed that after a drop of some 53% in the infiltration rate, affected by sealing the makeup air vent in one room, power consumption in that room decreased by some 20%. Consequently, limiting building infiltration rates should be sought in design and construction, and lately become mandatory by various energy codes either implicitly, as in Israel, or explicitly, as in Sweden. In Israel (SII 2003), this is accomplished by limiting the G-value (heat loss rate per unit volume of the design space and unit temperature difference [$W/m^3 \cdot K$]), which includes the contribution of the total air change rate. With accepted minimal insulation levels, the total infiltration rate is limited to approximately 1 ach or less. In Sweden (Mattsson 2006), a more direct step was taken, whereby the energy code requires that building envelope leakage rates do not exceed 0.8 $L/m^2 \cdot s$ (i.e., 2.88 $m^3/m^2 \cdot h$) under a pressure difference of 50 Pa. This requirement serves as a reference in the current investigation.

A literature survey indicated that, in general, although building envelopes seem to be much more airtight than windows and other openings, they are not completely airtight and may leak in the range of 0.03–10.35 ach under normal or extreme use conditions (Dumont et al. 1981; Kronvall 1978;

Rachel Becker *is an associate professor in the Faculty of Civil and Environmental Engineering, and Head of the Physical Performance of Buildings Division at the National Building Research Institute, Technion—Israel Institute of Technology.*

Nantka 1986; Offermann 1982; Sherman 1980; Yoshino et al. 1984). Most of these studies, however, have been performed in Northern European and North American cities, where construction is composed mainly of lightweight multilayered walls. In warmer countries, such as Israel and the entire Mediterranean region, thermal mass is more important and usually leads to masonry construction. Due to the mild winters, conduction heat loss does not justify multilayered construction, and the prevailing external walls are composed of a single layer of hollow-core concrete blocks (with either regular or lightweight-aggregate concrete), or autoclaved-aerated-concrete blocks.

The author performed an extensive literature survey, using the Engineering index for the period of 1970 to present, searching for data on air permeability of concrete block masonry construction. The following are the only sources that could be found.[1]

Svec and Goodrich (1986) measured temperature distributions across the height of two cavity block walls in an experimental basement facility. Insulation was always placed on the inside. They observed that convection within the cavity of a fully insulated wall caused a major drop in block surface temperature at the lower parts of the wall, with a very small temperature difference between the inner and outer surfaces of the block, reducing the soil/block interface temperature by some 4°C in comparison to the ground temperature at the same elevation. No data for block wall air permeability were reported.

Feldman et al. (1998) constructed a simple apparatus for measuring air infiltration through walls, and measured a brick wall. They do not describe the details of that wall, but their results indicate that infiltration is "very large" and reaches 4.5 L/m^2·min (0.27 m^3/m^2·h) under a pressure difference of 50 Pa, in comparison to 0.4 L/m^{2}min (0.024 m^3/m^2·h) for a gypsum sheathing board, and approximately 0.7 L/m^2·min (0.042 m^3/m^2·h) for the same brick wall when impregnated with paraffin.

Hosni et al. (1999) investigated the hygrothermal performance of concrete masonry walls under the hot and humid conditions of Brownsville, Texas. They measured air infiltration through 6 m^2 concrete block walls with various surface treatments. Their results indicated that under a reference pressure difference of 12.4 Pa, leakage rates for the untreated walls were in the range of 3.29–3.87 L/s (~2.0–2.3 m^3/m^2·h), and for the externally treated walls (by elastomeric stucco) they decreased to 1.16–1.35 L/s (~0.7–0.8 m^3/m^2·h). The hygric follow-up was for the same walls but with an interior finish composed of gypsum wallboard and an additional finishing layer. The walls without exterior finish accumulated more moisture under an interior latex finish. Walls with wallpaper accumulated extensive amounts of moisture, and no significant difference could be observed between the externally treated and nontreated walls. The authors do not describe the structure of the block. However, as this is the only test series on concrete block walls we could find in literature, its results serve as another reference for the current investigation.

The role of the built envelope in the total air permeability of buildings is enhanced by the fact that with the advent of the window manufacturing technology and the supervised testing that windows undergo in the framework of standard marking, these components became extremely airtight. In Israel, windows may contribute much less than 0.5 ach under normal conditions (Poreh 1992).

Consequently, it was evident that in order to address the effect of the built envelope on total building airtightness and the possible effect on its thermal performance, local data would have to be gathered. The current paper presents initial results obtained in the laboratory for three types of block walls used frequently in Israel according to climatic zone, as well as other preferences. In-situ measurements will be carried out at a later stage.

EXPERIMENTAL SETUP

The experimental study included air permeability testing and measurements that would allow the estimation of the thermal resistance of sections of block walls.

Three samples were tested: an autoclaved-aerated-concrete (AAC) block wall section, a hollow-core block wall section with regular-aggregate-concrete (HCRA) blocks, and a hollow-core block wall section with lightweight-aggregate-concrete (HCLA) blocks (with mixed pumice and scoria aggregates). AAC walls were built with 3 mm thin polymeric mortar, whereas HCRA and HCLA walls were built with regular 10 mm thick cementitious mortar. The net surface area of the tested walls was 1.25 × 1.25 m. The hollow-core blocks had three rows of cores, as shown in Figure 3. Exterior skins were 26 mm thick and internal skins 20–21 mm thick. All blocks had a 200 mm height and thickness, with each test wall extending six rows, thus including five internal horizontal joints and two wall-to-frame horizontal joints. The length of the HCRA blocks was 400 mm, and that of the other blocks was 500 mm, with each row including three or two-and-a-half blocks, respectively, with three vertical inner joints in each row and two wall-to-frame vertical joints. All of the wall-to-frame joints were sealed with foamed-in-place polyurethane. Typical construction of the walls is shown in Figure 1.

After construction, the walls were conditioned some 9 to 12 months in the open laboratory hall, where air temperature and humidity equal to approximately those of external ambient conditions without exposure to rain. Then they were tested for air permeability. The HCRA and HCLA walls have also

1. Surprised by the scarcity of publications on the subject, the author recognizes the fact that this survey might be incomplete, as the Engineering index includes only references to journal and conference papers and other well-documented international publications, but not to research reports published internally by various research bodies. However, as this paper is not intended to be a review paper, the risk that some additional information exists but was not detected by the author does not seem to be detrimental to the present findings.

Figure 1 *Typical construction of the wall specimens.*

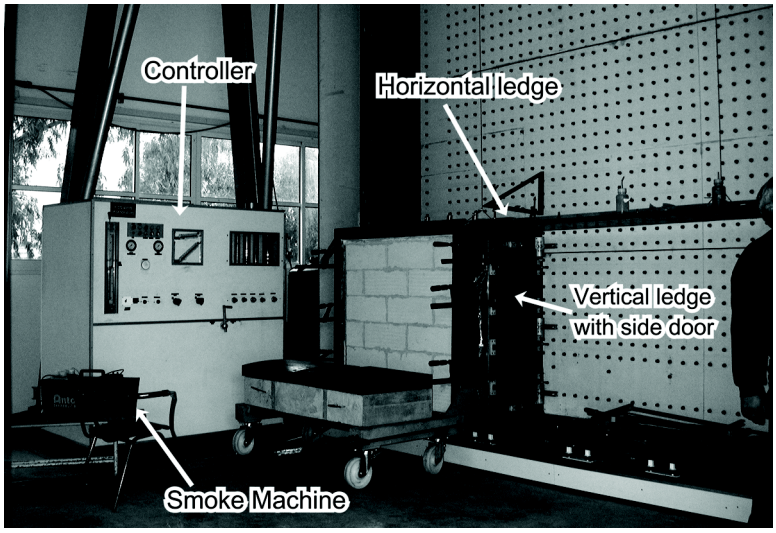

Figure 2 *Infiltration rate test assembly.*

been tested for thermal performance. After that, the HCRA wall was covered on the room-facing surface with a 3–5 mm cementitious brown coat (HCRA/BC), and the HCLA wall with a 10 mm lime-cement rendering on the chamber facing surface (HCLA/LCR). Both coatings were produced to meet the local standard SI 1920, Part 1 (SII 2000): cementitious brown coat (~1:2.5 [voluminal cement: natural sand] with ~350 kg cement per 1 m^3 final paste) and the lime-cement rendering (1:1:6 [voluminal cement: lime paste: natural sand] with ~180 kg cement per 1 m^3 final paste). After a 28-day conditioning period, the surface treated walls were retested for air permeability and thermal performance.

Air permeability was investigated by means of a K. Schulten "KS MSD-4040 Fenster Technique 1990" pressure box and controller, with a pressure difference capacity of 3000 Pa and a 210 m^3/h airflow range. Pressure and infiltration rates are indicated by means of liquid meniscus locations in relevant manometer U-tubes. The resolution of readings is: ±0.5 Pa for the pressure range of 150 Pa, ±2.5 Pa for the pressure above 150 Pa, ±0.05 m^3/h for infiltration rates below 2.4 m^3/h, ±0.1 m^3/h for infiltration rates up to 10 m^3/h, and ±1.0 m^3/h for infiltration rates above 10 m^3/h. Zeroing of all manometers is performed before every test. The test chamber is created within the box facility by means of movable upper and side ledges. The ledges are firmly secured and pressed to the frame of the box and sealed along the perimeter. Prior to its assembly, the test wall was covered by a thick polyethylene sheet and leakage spots between the wall specimen and the chamber, as well as between the ledges and the frame of the box, all were identified by means of white smoke. When no more smoke was emitted, the pressure was gradually increased up to 500 Pa, and the chamber leakage rate was monitored. After releasing the pressure, the polyethylene sheet was cut out (entering the chamber through its side door) along the inner circumference, and the pressure was gradually increased again, now monitoring the gross leakage rate of the wall. The net leakage rate of the wall was then derived from the differences between the two data sets, as explained in the results section. The general test assembly is shown in Figure 2.

Thermal measurements were performed in a temperature- and humidity-controlled laboratory room with setpoint conditions: 18°C/53%. The room is 3.45 m wide, 7.45 m long, and

2.95 m high and located in the basement of the National Building Research Institute. Ventilation air enters the room through uniformly distributed four 0.15 × 0.90 m grilled inlets along the top of one side-wall. Room air is extracted through an outlet located in the rear of the room at the bottom of the other side-wall. All the basement laboratory rooms are continuously controlled by means of a central system, which enables individual temperature and humidity setpoints for each laboratory. The temperature in the corridor connecting the laboratories is continuously controlled as well, with a constant 21°C setpoint. The room is separated from the other laboratories by a 0.2 m concrete wall covered on the room-facing side by a 100 mm foamed polyurethane layer and 15 mm facing plywood boards. The walls separating it from the corridor are composed of hollow-core concrete blocks. An insulated box, which meets the requirements of the Israeli Standard SI 1375 (SII 1999) stands on four wheels in the rear side of the room along the room centerline with a distance of 0.9 m from each side wall, 1.7 m from the rear wall, and 0.3 m above the floor. The box has five walls composed of continuous 175 mm foamed polyurethane sandwiched between two 15 mm plywood boards (surface to surface thermal resistance of each section ~6.0 m^2·K/W and free of thermal bridges except around the front opening) and a square 1.25 × 1.25 m vertical opening. The inner width and height of the box are 1.25 m and its depth is 0.9 m. A flexible 130 × 30 mm polyethylene foam band is glued around the opening on the front edge of the box frame, so that it would be squeezed between the specimen frame and the box frame upon clamping the wall specimen to the box. A 25 W incandescent bulb is used as the inner box heater and is mounted within an aluminium foil cone on the box symmetry plane at a 0.45 m distance from the rear box wall and 0.12 m above the box floor. The cone is closed at its top and open at the bottom. A 1300 rpm 5–33 W fan is mounted on the box symmetry plane 0.2 m from the rear wall and 0.13 m below the box ceiling at a 45° angle toward the rear wall. This setup is stipulated by the Standard SI 1375 (SII 1999) in order to provide a uniform temperature on the surface of a uniform reference specimen plane. Periodic tests of the box by means of the uniform polymeric reference specimen are performed to ensure the uniform temperature distribution (differences between the center of the board and any of the four corners do not exceed ±0.1°C and are nonmonotonic).

For the current tests, in order to create a pressure difference across the wall specimen, a one way 550 L/h pump was connected to the box. A flexible hose that penetrates the box wall can suck the air at the geometric center of the box. A low leakage valve along the hose ensures the box airtightness when the pump is not in operation. The constancy of the airflow delivered by the pump was not given by the manufacturer and was not established experimentally.

Before connecting any wall specimen to the box, the specimen had been conditioned in the test room for a few days, until measurements showed that a steady-state and uniform temperature has been achieved throughout its cross section (temperature fluctuations between consecutive measurements taken at one-hour intervals, as well as between any two adjacent points did not exceed ±0.1°C and were nonmonotonic). After clamping the specimen to the box, the entire visible surface of the specimen frame was covered by 150 mm thick flexible foamed polyurethane mattresses to reduce transverse heat flow and ensure that the main heat flow is perpendicular to the block-wall plane. Once the box heater and fan were running at full capacity, they supplied a constant source of power for the entire test period. The box-side surface of the wall specimen was thus exposed to the warm air and the room-side surface to the steadily cool ambient air. This setup created automatically a transient period (lasting between 40 to 50 hours) until steady state was reached within the box and throughout the wall (practically achieved steady-state has been defined when temperature fluctuations between consecutive measurements of box air temperature and at any given point in the specimen, taken at one-hour intervals, did not exceed ±0.1°C and were obviously nonmonotonic).

Temperature distribution was monitored continuously by means of ground shielded 4 m full length ANSI Standard Gauge 24 type T thermocouples (TCs), with a 0.508 mm nominal conductor thickness. Readings were taken by means of a WaveTek Model 52A data logger with a Model 53 I/O expansion. The declared manufacturer accuracy for type T TCs is: ±0.2°C, but the stability of readings during steady-state, as well as previous calibration of TCs with the same data logger indicate that the actual accuracy is better than the declared one. Exposed TC junctions were twisted and tightly attached to the surface by a 15 × 15 mm reflective aluminium foil that served for radiation protection as well. The TCs that measured the room and box air temperatures were placed inside a reflective foil conic cylinder to reduce the effects of radiation. The TCs were positioned in the air 0.1 m from the center of the block specimen. Three TCs were glued along the height on every surface of two typical block cross sections of a single block, and at the central and side-cross sections of the block, as shown in the Figure 3. In the HCRA block, the side cross section includes two cores, while the central cross section includes only one core. In the HCLA block, the side cross section includes one core, while the central cross section includes two cores. TCs were glued on the room and box facing surfaces, as well as on all core facing surfaces in the two cross sections of every wall. In addition, room and box air temperatures were also measured continuously. Altogether, 32 TCs were included in every test (without any redundant TCs), with the first channel used also for the cold junction compensation. Measurements at all points were taken every 15 minutes during the transient period and every 60 minutes during steady state. The average of five successive readings taken at one-second intervals was recorded as the temperature at the given time.

Pressure difference between the warm and cool sides of the wall was monitored by means of a Setra differential pressure transducer, with a bidirectional pressure range of

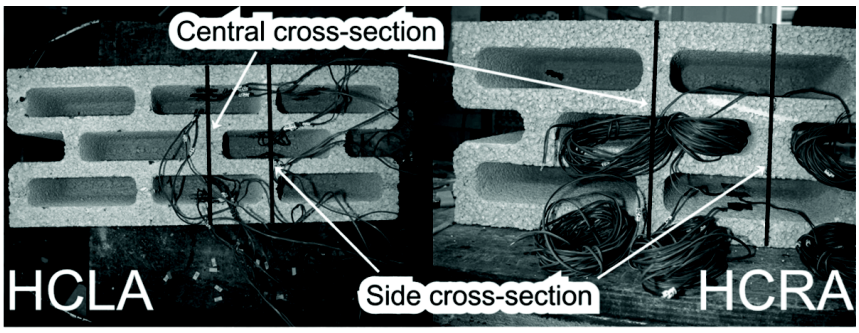

Figure 3 *Thermocouples assembly within the cores of the HCRA and HCLA blocks.*

±63.5 Pa (Poreh 2004) and ±0.04% accuracy of voltage reading. The estimated error of the calibrated pressure readings is ±1.5% of reading.

Once steady state was practically achieved (i.e., the temperatures measured on the block remained essentially constant for at least 48 hours), the temperatures were averaged over a 24-hour period. The pressure was averaged over the same period.

Then the pump valve was opened and the pump was activated, extracting air from the box at a maximal rate of 0.35 $m^3/m^2/h$. Cool room air was thus sucked into the wall specimen through its entire surface area, but the uniformity of the flow across the specimen surface could not be assessed. Flow reversal was not possible by this setup. At the maximal rate it may take mostly 34 minutes for the air to flow through the wall. After a transient period of less than 48 hours, a new steady state had been established. Pump operation and monitoring continued until the new steady state had been practically achieved (i.e., the temperatures measured on the block remained essentially constant for at least 48 hours). The temperatures and pressure were averaged over a 24-hour period.

RESULTS AND DISCUSSION

Air Permeability

The air leakage rate of the test chamber was plotted versus the pressure difference. Nonlinear least-squares regressions showed that it is best approximated by a cubic polynomial. Typical leakage of the chamber was less than 1.00±0.05 m^3/h under a pressure difference of 50 Pa (< 0.64 m^3/m^2h at 50 Pa), and less than 5.7 ± 0.1 m^3/h under a pressure difference of 500 Pa (<3.7 m^3/m^2h at 500 Pa). The net wall permeability of each sample was thus obtained by deducting the values obtained from the relevant polynomial from the gross measurement values of that wall.

For the AAC wall section the gross leakage rate up to 65 Pa was identical to that of the chamber (0.75 ± 0.05 m^3/h at 65 Pa), indicating an almost zero (0.00 ± 0.07 m^3/h) leakage rate within this range. Above 65 Pa the gross leakage rate of the wall exceeded that of the chamber. At 500 Pa the gross wall reading was 3.8 ± 0.05 m^3/h, while that of the chamber was 2.8 ± 0.05 m^3/h, indicating a net leakage rate of 1.0 ± 0.07 m^3/h (e.g., 0.64 ± 0.04 $m^3/m^2{\cdot}h$ at 500 Pa).

On the other hand, much larger net leakage rates have been measured for the hollow-core block walls, in both their bare as well as surface treated configurations. Due to the large leakage rates of the HCRA and HCLA samples, their tests were terminated after reaching a pressure difference of 150 Pa and 200 Pa, respectively. The AAC sample was actually tested up to 600 Pa.

For the hollow-core blocks, net wall permeability has been approximated by means of the exponential expression (Etheridge 1977; Sherman 1980),

$$q_{air} = A \cdot \Delta p^n , \qquad (1)$$

where

q_{air} = infiltration rate per unit area (m^3/m^2h),
Δp = pressure difference across wall (Pa), and
A, n = parameters.

Due to the zero net infiltration rate observed for the AAC sample up to 65 Pa, the exponential representation could not be used for this wall.

Figure 4 shows results of the net infiltration rate per unit wall area for all the five wall specimens, and the exponential trend lines for the four hollow-core block wall specimens.

Table 1 shows the derived values of n and A, as well as the goodness of fit correlation coefficient R^2 and the ψ-test between the measured values and those expected according to Equation 1, for the four hollow-core block wall samples within the range of 150 Pa. The statistical tests indicate that despite local differences between calculated and measured values that can be as large as 18% (for HCLA/LCR at 70 Pa), the approximation of the measured data by the exponential line is very good. Apparently, the values of the exponent n for the highly permeable walls HCRA and HCLA were 0.83 and 0.79, respectively, and the parameters A were 1.63 and 1.53, respectivley. The cementitious brown coat reduced the exponent n to 0.61, and the A parameter to 0.11, whereas the internal lime-cement rendering hardly altered the exponent and only reduced the A parameter to 0.04. According to literature,

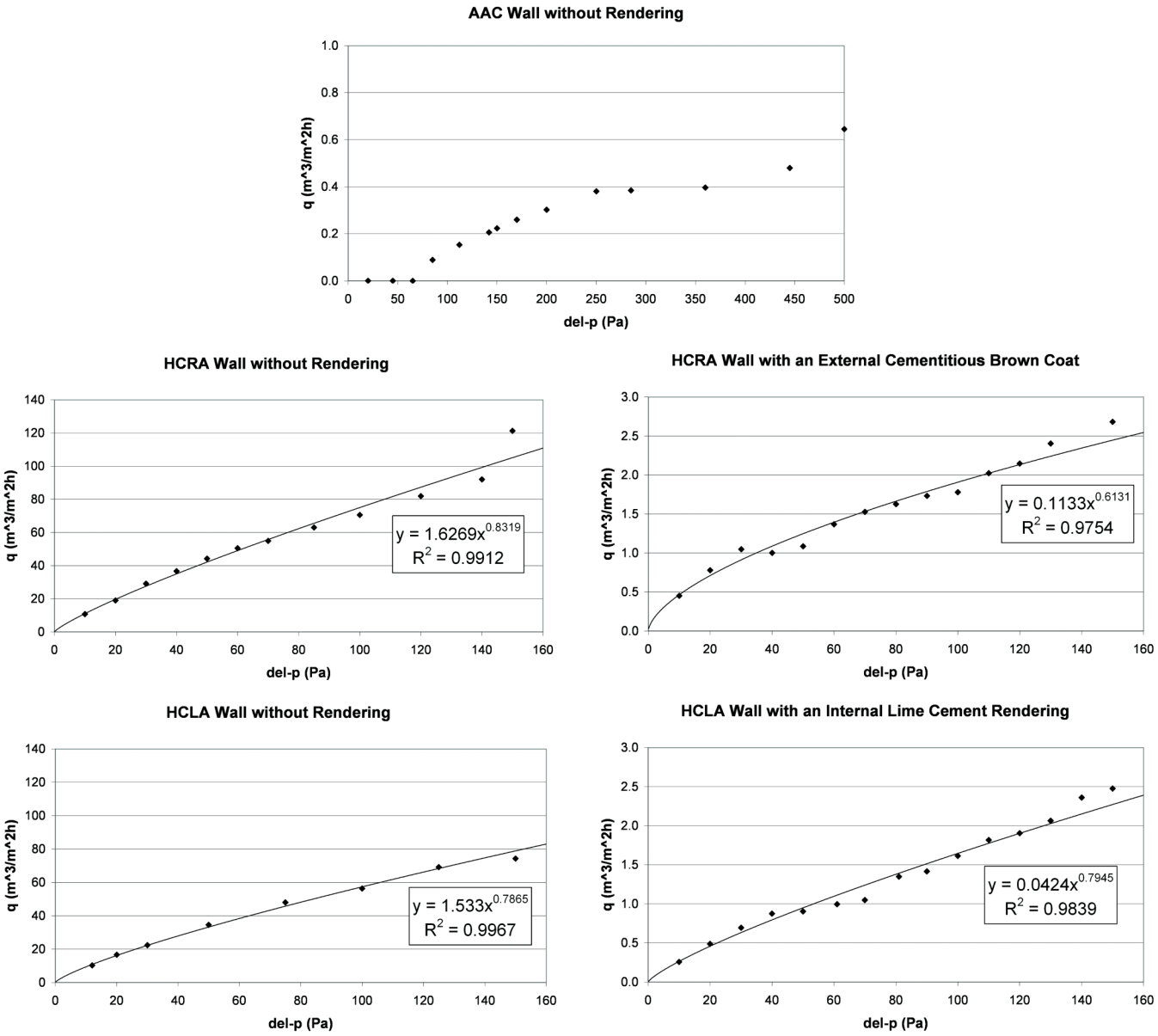

Figure 4 *Air permeability results for the various samples.*

(Sherman 1980; Hagentoft 2001), $n \approx 1.0$ indicates laminar flow, whereas $n \approx 0.5$ indicates turbulent flow. Due to the lack of fine aggregates in the block concrete fabric, pores are larger than those in regular cementitious or lime-cement pastes. It thus may seem that airflow in the larger pores of the bare walls is more laminar than that in the finer pores of the cementitious brown coat. This observation deserves further investigation, but was not pursued at this stage.

Table 1 includes also the measured infiltration rate at 50 Pa, q_{50} and at 150 Pa, q_{150} for all the five samples. When comparing the measured q_{50} results to the Swedish code stipulation (limit leakage rate of 2.88 m^3/m^2h at 50 Pa), it is seen that the bare HCRA and HCLA walls infiltrate more than 15 and 12 times that value, respectively. However, the application of either surface coating, the thin external brown coat or the thicker internal lime cement rendering, reduces air permeability to an extent that exceeds that requirement by a factor of more than two.

Infiltration rates under a 50 Pa pressurization test, as well as for natural infiltration (wind pressure on the given surface) under a pressure difference of 50 Pa (wind speed ~9 m/s) and 150 Pa (wind speed ~15.5 m/s), were computed for a typical 100 m^2 ($V = 250$ m^3) Israeli dwelling that has usually external walls on two sides at least. For such a dwelling, the net concrete block wall area (excluding windows, doors and reinforced concrete structural members) would be approximately 16.6 m^2 on the front side, A_f, and 19.6 m^2 on the transverse side, A_t. The various air change rates were obtained by the

Table 1. The Parameters n and A in Equation 1 and the Measured Infiltration Rates at 50 Pa, q_{50} and at 150 Pa, q_{150} for the Various Block Walls ($m^3/m^2/h$)

Wall Type	AAC	HCRA	HCRA/BC	HCLA	HCLA/LCR
n		0.8319	0.6131	0.7865	0.7945
A		1.6269	0.1133	1.533	0.0424
R^2		0.9912	0.9754	0.9967	0.9839
ψ-test		0.9676	1.0000	0.9985	1.0000
q_{50}	0.00 ± 0.04	44.20 ± 0.90	1.09 ± 0.04	34.56 ± 0.90	0.90 ± 0.04
q_{150}	0.22 ± 0.04	121.33 ± 0.90	2.68 ± 0.08	74.24 ± 0.90	2.46 ± 0.08

Table 2. Estimated Air Change Rates (ach), N, for Various Situations in a Typical Dwelling

Wall Type	AAC	HCRA	HCRA/BC	HCLA	HCLA/LCR
50 Pa pressurization	0.0	6.4	0.16	5.0	0.13
50 Pa across front wall	0.0	2.9	0.07	2.3	0.06
50 Pa across side wall	0.0	3.5	0.09	2.7	0.07
150 Pa across front wall	0.01	8.1	0.18	4.9	0.16
150 Pa across side wall	0.02	9.5	0.21	5.8	0.19

following equations, using the measured infiltration rates, q_p, that were obtained under the relevant pressure difference p.

For the 50 Pa pressurization test,

$$N = q_{50} \cdot (A_f + A_t)/V. \quad (2)$$

For the natural infiltration under a given pressure difference p across the front wall,

$$N = q_p \cdot A_f/V. \quad (3)$$

For the natural infiltration under a given pressure difference p across the transverse side wall,

$$N = q_p \cdot A_t/V. \quad (4)$$

The results are given in Table 2.

The estimated all dwelling infiltration rates for the bare hollow-core block walls are extremely high and would not meet any energy saving criteria, which would usually limit the unwanted air change rate through walls to less than 0.1 ach. The application of the external brown coat or internal lime cement rendering may reduce the infiltration rates, but meet the above-mentioned criterion only when natural infiltration at medium wind speeds (indicated by p = 50 Pa) occurs. On the other hand, the estimated all dwelling infiltration rates for the bare AAC walls is extremely low and meets this criterion at both pressure levels with a large margin of safety.

As mentioned in the Introduction, due to lack of available results from literature, infiltration rates obtained here could be compared only to those obtained by Hosni et al. (1999). As they measured block wall samples at the unique pressure difference of 12.4 Pa, infiltration rates of the current hollow-core blocks under this pressure difference were computed using the relevant n and A values shown in Table 1. For the bare blocks, the infiltration rates of the currently tested wall specimens were five to six times larger than those obtained by Hosni. On the other hand, for the surface treated walls, infiltration rates of the currently tested wall specimens were some 40% to 70% of those obtained by Hosni.

Thermal Performance

For all of the walls, the first stage of steady state has been practically reached less than 48 hours after activating the box heater and fan. A 24-hour average temperature difference of 10.0°C, 9.7°C, 11.7°C, and 11.7°C was maintained between the air temperatures on the warm (facing the box) and cool (facing the room) sides of the HCRA, HCRA/BC, HCLA, and HCLA/LCR specimens, respectively. Under steady-state conditions, temperature fluctuations between any two measurements made at 1-hour intervals did not exceed 0.1°C and were not monotonic. The standard deviation of temperature fluctuations over a 24-hour period for all the measurement points was as follows: for HCRA: 0.03°C to 0.11°C, for HCRA/BC: 0.00°C to 0.05°C, for HCLA: 0.00°C to 0.06°C, and for HCLA/LCR: 0.00°C to 0.05°C. The temperature difference between the top and bottom TCs along the height of the various surfaces was usually small, with the largest differences observed in all cases on the room-side surface in the core. The absolute differences in the 24-hour steady-state averages between the top and bottom of this surface were: for HCRA: 0.53°C, for HCRA/BC: 0.36°C, for HCLA: 0.47°C, and for HCLA/LCR: 0.40°C. However, during the transient period, and mainly during the initial period of several hours after activating the box heater and fan, the temperature at any point in the HCRA and HCLA blocks exhibited much larger

fluctuations when compared to the behavior of the HCRA/BC and HCLA/LCR blocks. Figure 5 shows temperature evolution results for the central cross section of the HCRA and HCRA/BC blocks during the initial transient period of 5 hours and during a steady-state period of 30 hours.

Throughout the transient period, the variation of the temperatures along the height of any given surface of the highly permeable HCRA block is larger than that of the surface-treated air tighter HCRA/LCR block. Moreover, for a given surface of the HCRA block, the locations of the warmest and coldest points in the blocks vary continually during the initial five-hour period. The temperature difference between the top and bottom of each of the monitored surfaces was computed for every measurement during the initial five-hour transient period. Maximum statistical spatial variation in each specimen, defined as twice the standard deviation, along with the minimum and maximum observed spatial temperature differences are as follows: 0.75°C (–0.5°C to 1.2°C), 0.40°C (–0.7°C to 0.0°C), 0.15°C (0.0°C to 0.3°C) and 0.16°C (0.0°C to 0.2°C), for the HCRA, HCLA, HCRA/BC and HCLA/LCR, respectively.

The fluctuations of the temperatures with time during the initial warming period of the HCRA and HCLA specimens can be attributed to some convective currents within the bare block, which exist even when no active pressure difference is induced across the wall, and probably do not exist in the blocks with the tight surface.

In addition, during the initial warming period, the temperature rise at all of the surfaces of the HCRA wall is faster than that of the HCRA/BC wall, with times of temperature propagation some 30–120 minutes shorter. A significant observation is that the rate of temperature rise is larger even in the room side of the wall.

Regarding the dynamics of the wall when exposed to weather-related fluctuations with time periods of several hours and negligible pressure differences across the wall, the above observation may imply that the room side surface of the permeable wall may respond faster to the external ambient temperature changes when compared to a much tighter wall, thus warming up faster in the morning and cooling down faster in the evening. These indications deserve further investigation under cyclic dynamic conditions resembling typical diurnal changes.

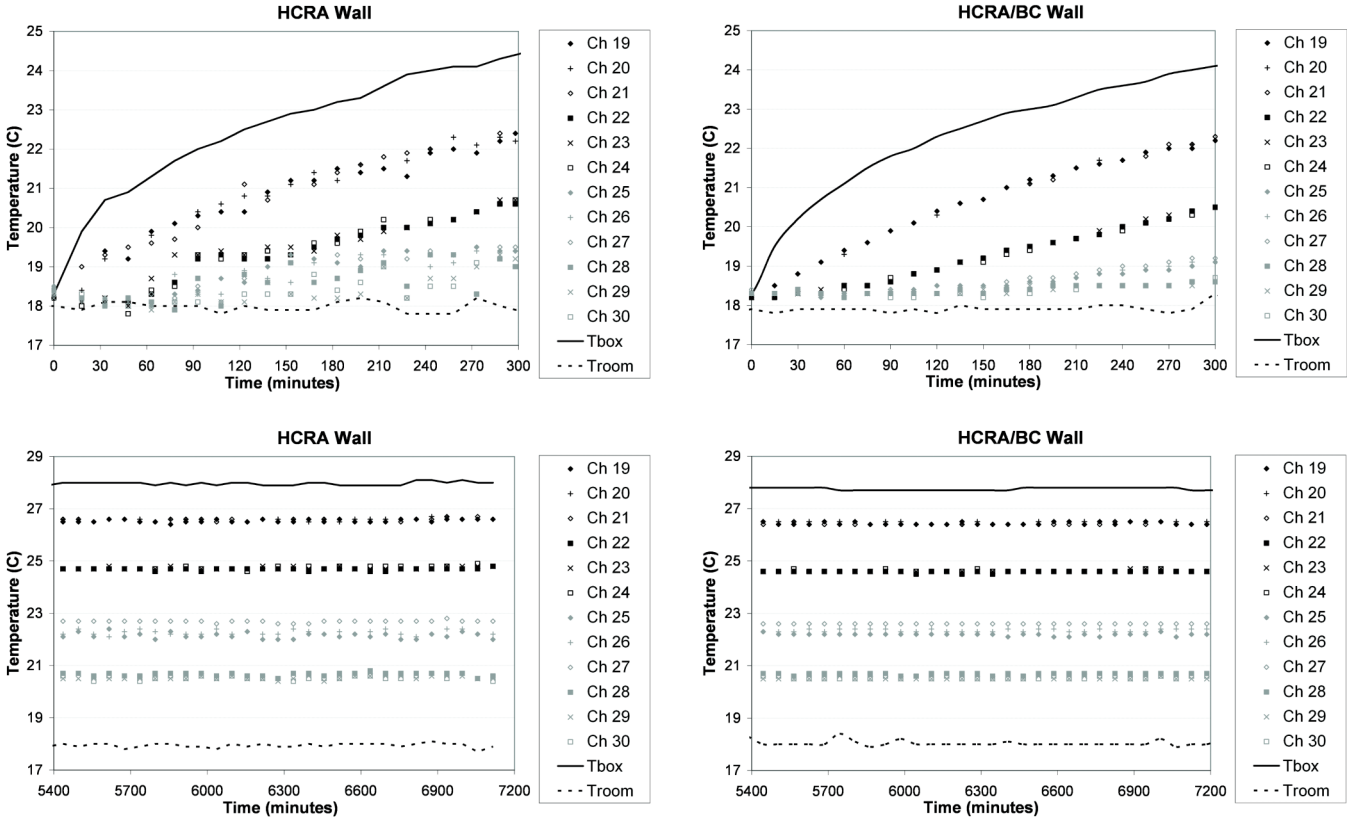

Figure 5 *Temperature evolution in the central cross section of HCRA and HCRA/BC blocks during the initial five-hour period and during steady state. Point locations: Ch19-Ch21—box facing surface, Ch22-Ch24—box-side surface in core, Ch25-Ch27—room-side surface in core, Ch28-Ch30—room-facing surface. The smallest channel number in every group signifies the upper TC and the largest number the lower TC.*

After the completion of the 48-hour steady-state period for steady-state heat flow measurements, the air pump was activated and a pressure difference causing a maximal flow of 0.35 m^3/m^2h was induced from the room side to the box. The heat flow reached a new equilibrium in less than an additional 48 hours. The increase in the pressure differences across the walls were as follows: for the bare HCRA and HCLA specimens were 0.1±0.0015Pa and 0.3±0.0045Pa, respectively, whereas for the coated HCRA/BC and HCLA/LCR specimens were 0.8±0.012Pa and 1.0±0.015Pa, respectively. Although very small, this airflow also reduced the 24-hour average temperature difference between the box and room air by 0.2°C ± 0.14°C for the HCRA and HCRA/BC specimens and by 0.1°C ± 0.14°C for the HCLA and HCLA/LCR specimens, with an identical effect on the difference between the box-side block surface temperature and the room air, indicating that in winter even small pressure differences that allow a small airflow of colder air through external walls may reduce their internal surface temperature. These results are in general agreement with the observations and analysis made by Taylor and Imbabi (1997) for walls designed under the concept of dynamic insulation.

To estimate the effect of the block air permeability on heat flow through the wall and on the apparent thermal resistance, the heat transfer coefficient of the cold room-side surface film, h_{sr}, of the block wall specimens was estimated.

Since the cold room is kept continuously at a constant air temperature and its walls are of heavyweight construction, the differences between the inner cold room surface temperatures and the cold room air temperature are very small. Typical 24-hour average differences and their standard deviations (in parentheses) are: 0.71(±0.10)°C for the side walls, 1.79(±0.11)°C for the ceiling, 0.46(±0.08)°C for the floor, and 0.3(±0.10)°C for the door in the wall facing the wall specimen. As the cold room surface temperatures have not been measured continuously during the entire period of the tests, the radiant heat transfer coefficient, h_{rsr}, of the block-wall specimen surface film on the cold room-side is estimated by Equation 5, assuming negligible effect of the room walls:

$$h_{rsr,j} = 4 \cdot \varepsilon \cdot \sigma \cdot T_{ra,j}^3 \quad (5)$$

where

$h_{rsr,j}$ = the radiant heat-transfer coefficient of the surface film on the cold room-side of the specimen at block cross section j, $W/m^2 \cdot K$

ε = 0.9, emissivity of all the surfaces and other objects in the room

σ = $5.67 \times 10^{-8} W/m^2 \cdot K^4$, Stefan Boltzmann constant

and

$$T_{ra,j} = \frac{T_r + T_{sr,j}}{2} + 273.15 \quad (6)$$

where

T_r = room air temperature measured in front of the specimen, °C

$T_{sr,j}$ = average room-side surface temperature along the block cross section j, °C

As aforementioned, the measured surface temperatures of the cold room walls, ceiling, and floor were somewhat larger than the room air, implying that the value of h_{rsr} is somewhat larger than that predicted when T_{ra} is given by Equation 6. To estimate the upper bound of h_{rsr}, an environmental temperature that is 1.5°C larger than T_r was used in Equation 6.

The average air velocity in front of the cold room-side surface of the HCLA/LCR specimen was measured at a distance of 0.1 m from the specimen surface when the pump was not activated by means of a Kurz Instruments hot-wire anemometer, with a range of 0 to 0.508 m/s and a ±0.015 accuracy. Typical 24-hour average values and their standard deviations (in parentheses) are: 0.118(±0.0028) m/s in the vertical direction, 0.065(±0.0068) m/s in the horizontal direction, 0.134(±0.0044) m/s for the vector sum of the velocities in the plane parallel to the specimen surface, and 0.001(±0.0000) m/s perpendicular to the specimen.

The square root of the Grashof number, Gr, for the cold room-side surface of all the specimens was between 22900 to 27500 throughout the entire test period. The Reynolds number for the 1.25 m specimen height and a 0.15 m/s air velocity (rounded value for the measured 0.134 m/s) is ~12500, which indicates that the cold room-side boundary layer flow may be laminar but not stable. The Richardson number under these circumstances is larger than 3, which indicates that natural convection likely dominates in the cold room-side boundary layer (Kobus and Wedekind 1996). Thus, although the velocity of 0.134 m/s is almost half of the 0.3 m/s velocity stipulated by ASTM 1363 (ASTM 2005) for forced convection, the paper has not considered the possibility of combined forced and natural convection on the cold room face of the wall specimens. The Davies formulation (Davies 2004) has then been used for estimating the convective heat transfer coefficient, h_{csr}, of the block-wall specimen surface film on the cold room-side:

$$h_{csr,j} = 0.6 \cdot (\lambda_{air} \cdot \rho_{air} \cdot Cp_{air})^{0.5} \cdot \left(\frac{\Delta T_{sr,j} \cdot g}{H \cdot \beta}\right)^{0.25} \quad (7)$$

where

$h_{csr,j}$ = convective heat-transfer coefficient of the surface film on the cold room-side of the specimen at block cross section j, W/m^2K

β = expansion coefficient of air, calculated by $1/T_{ra}$, K^{-1}

λ_{air} = thermal conductivity of air, W/m·K

ρ_{air} = air density, kg/m^3

Cp_{air} = air specific heat, J/kg·K

and

$$\Delta T_{sr,j} = T_{sr,j} - T_r \quad (8)$$

The estimated value of the total heat-transfer coefficient of the cold room-side surface film at cross section j, $h_{sr,j}$, is then given by

$$h_{sr,j} = h_{rsr,j} + h_{csr,j}. \quad (9)$$

The aerial rate of heat flow from the box into the room through the block at cross section j, $q_{Tsr,j}$, is estimated by

$$q_{T_{sr,j}} = h_{sr,j} \cdot \Delta T_{sr,j}. \quad (10)$$

The apparent thermal resistance (air to air) at cross section j, $R_{es,j}$, is estimated by

$$R_{es,j} = \frac{T_b - T_r}{q_{T_{sr,j}}}, \quad (11)$$

where

T_b = box air temperature, °C.

In literature, there are several other equations for the estimation of the convective heat transfer coefficient of the surface film, h_{cs}. The minimal and maximal values of h_{cs} have thus been calculated by the following Equations 12 and 13, as listed in the extensive literature survey performed by Khalifa (2001).

$$h_{csr,j,min} = 0.48 \cdot \mathrm{Gr}_j^{0.25} \quad (12)$$

$$h_{csr,j,max} = 1.973 \cdot \Delta T_{sr,j}^{0.25} \quad (13)$$

The estimated possible range for the estimated value of R_{es} has been calculated for the range of h_{csr}, as defined by Equations 12 and 13.

The 24-hour averages of estimated h_{csr}, h_{sr}, q_{Tsr}, and R_{es} values during the steady-state periods for the side and central cross sections are given in Table 3, including the estimated possible ranges of h_{csr}, h_{sr}, and R_{es}. Under the given assumptions, the ranges of the total surface heat-transfer coefficient, h_{sr}, for all the four walls are within the bounds 6.59–7.69 W/m^2·K, which are 9% to 21% below the commonly used engineering value of 8.33 W/m^2·K.

The results indicate that during the pump activated period, the estimated heat flow rate through every specimen was smaller than that calculated for the first steady-state period, with reductions between 1% to 3.5%. However, as mentioned before, despite the reduced outgoing heat flow, the box air temperature could not be kept at its previous level but rather decreased slightly, apparently due to the energy that went into heating the incoming cooler air. The estimated R-values and their possible ranges are almost identical during the two steady-state periods, and no consistent change could be observed due to the small pressure difference across the specimens, whereas the estimated lower values of R_{es}, which were

Table 3. Estimated Values of Cold Room-Side h_{csr}, h_{sr} (W/m^2·K), q_{Tsr} (W/m^2), and R_{es} (m^2·K/W) Obtained at the Side and Central Cross Sections of the Hollow-Core Blocks when the Air Pump was Off and On Assuming Natural Convection in the Boundary Layer

		HCRA		HCRA/BC		HCLA		HCLA/LCR	
	Air Pump Flow	Side Cross Section	Central Cross Section	Side Cross Section	Central Cross Section	Side Cross Section	Central Cross Section	Side Cross Section	Central Cross Section
h_{csr} (1) (range)	Off	1.69 1.59–2.43	1.74 1.64–2.50	1.70 1.60–2.45	1.74 1.63–2.49	1.65 1.55–2.36	1.61 1.51–2.31	1.63 1.53–2.34	1.59 1.50–2.30
h_{sr} (range)	Off	6.79 6.69–7.61	6.85 6.74–7.69	6.80 6.70–7.63	6.85 6.74–7.68	6.73 6.63–7.52	6.68 6.59–7.47	6.74 6.64–7.53	6.70 6.61–7.48
q_{Tsr}	Off	15.8	17.8	16.1	17.5	13.8	12.6	13.3	12.3
R_{es} (2) (range)	Off	0.64 0.57–0.65	0.57 0.50–0.57	0.61 0.54–0.61	0.56 0.50–0.57	0.84 0.76–0.86	0.93 0.83–0.94	0.88 0.78–0.89	0.95 0.85–0.96
h_{csr} (1) (range)	On	1.69 1.59–2.43	1.73 1.62–2.48	1.69 1.59–2.43	1.73 1.62–2.48	1.64 1.53–2.34	1.59 1.50–2.29	1.63 1.53–2.33	1.59 1.50–2.29
h_{sr} (range)	On	6.80 6.70–7.62	6.85 6.74–7.68	6.80 6.70–7.62	6.84 6.73–7.67	6.72 6.61–7.50	6.67 6.59–7.45	6.74 6.64–7.52	6.69 6.60–7.47
q_{Tsr}	On	15.6	17.2	15.7	17.0	13.4	12.2	13.2	12.1
R_{es} (2) (range)	On	0.63 0.56–0.64	0.57 0.51–0.58	0.61 0.54–0.62	0.56 0.50–0.57	0.86 0.77–0.88	0.95 0.85–0.96	0.87 0.78–0.89	0.95 0.86–0.97

Notes:
(1) The numbers in the second row indicate the estimated possible range of h_{csr}.
(2) The numbers in the second row indicate the estimated possible range of R_{es} due to the possible range of h_{csr}.

obtained using $h_{sr,max} = h_{csr,max} + h_{rsr,max}$, are some 10% lower than the values derived by h_{csr} that were calculated by Equation 7, and the estimated upper values, which were obtained using $h_{sr,min} = h_{csr,min} + h_{rsr}$, are less than 2% larger.

On the other hand, during the initial five-hour transient heat flow period after activating the heater and fan in the hot box, the estimated heat flow rate, q_{Tsr}, was much smaller than that at steady state, and the estimated apparent thermal resistance was much larger, with estimated R-values more than twice those obtained at steady state. These results indicate that under actual ambient conditions, which in the Mediterranean weather are far from steady state, concrete block walls may perform much more efficiently than expected on the basis of steady-state R-values during external ambient temperature decreases in winter as well as during external ambient temperature increases in summer, while the overall daily energy performance may be hardly affected due to poorer performance when ambient temperature increases in winter and decreases in summer. This observation deserves further investigation, which should be carried out under well-controlled dynamic conditions simulating diurnal oscillations of the external air temperature and various indoor air temperature control schedules.

Addressing the entire set of results, it is finally deduced that from an energy-saving viewpoint, and in order to fully utilize the thermal efficiency of massive block walls, their air permeability should be limited in order to minimize the energy required for heating the infiltrating air in winter and cooling it in summer. A reasonable limit is an infiltration rate that can ensure a contribution to a total-dwelling leakage rate that does not exceed 0.1 ach. Results for the specimens tested here indicate that for medium wind speeds, this can be accomplished by means of a brown coat applied on the exterior surface, or by means of the interior regular lime cement rendering. Apparently, a combination of the two improves airtightness, but this has not been tested yet at the time of finalizing this paper.

CONCLUSIONS

Air permeability of three 1.25 × 1.25 m block wall sections was measured in the 0–200 Pa range by means of a pressure box. Specimens included autoclaved aerated blocks, AAC, regular aggregate concrete hollow-core blocks, HCRA, lightweight aggregate hollow-core blocks, HCLA, the HCRA wall with a cementitious brown coat on the cold side, HCRA/BC, and the HCLA wall with a lime cement rendering on the warm side, HCLA/LCR. Voluminal infiltration versus pressure difference was approximated by an exponential line, with a parameter A and exponent n. Results were extrapolated to evaluate the air change rate (ach) in a standard 100 m^2 dwelling. The main conclusions of this part are as follows:

1. Autoclaved aerated concrete block wall specimens proved to be extremely airtight, with almost zero (0.00 ± 0.045 m^3/h) leakage rate within the initial 65 Pa range. At 500 Pa, the net leakage rate was 0.64 ± 0.04 $m^3/m^2 \cdot h$. Estimated infiltration rates for the standard 100 m^2 dwelling were 0.01–0.02 ach under a pressure difference of 150 Pa.
2. Specimens HCRA and HCLA were highly permeable, with 50 Pa leakage rates of 44.20 ± 0.90 $m^3/m^2 \cdot h$ and 34.56 ± 0.90 $m^3/m^2 \cdot h$, respectively. The exponential approximations for these specimens were $1.63e^{0.83}$ and $1.53e^{0.79}$, respectively. Estimated infiltration rates for the standard 100 m^2 dwelling were ~2–6 ach under a pressure difference of 50 Pa, and ~5–10 ach under a pressure difference of 150 Pa.
3. The application of an external 3 mm cementitious brown coat reduced infiltration rates significantly, leading to a 50 Pa leakage rate of 1.09 ± 0.04 $m^3/m^2 \cdot h$, and estimated infiltration rates for the standard 100 m^2 dwelling of 0.07–0.16 ach and 0.18–0.21 ach under pressure differences of 50 Pa and 150 Pa, respectively. The exponential approximations for this specimen was $0.11e^{0.61}$. Further research is needed to understand why the application of the external cementitious brown coat, which has finer pores than the block-concrete fabric, has reduced the exponent in comparison to the HCRA specimen, indicating a more turbulent air flow regime in the finer pores.
4. The application of an internal regular 10 mm lime-cement rendering reduced infiltration rates in a similar manner, leading to a 50 Pa leakage rate of 0.90 ± 0.04 $m^3/m^2 \cdot h$, and estimated infiltration rates for the standard 100 m^2 dwelling of 0.07–0.13 ach and 0.16–0.19 ach under pressure differences of 50 Pa and 150 Pa, respectively. The exponential approximations for this specimen was $0.04e^{0.79}$, with essentially no change in the exponent in comparison to the HCLA specimen.

Thermal performance of the hollow-core specimens was measured by means of a heated insulated box located in a cold room. Thermal resistance of the two representative cross sections was estimated by comparing temperature differences across specimens to estimated room-side surface resistances. After steady state was reached, an air pump was activated to induce small pressure differences (0.1–1.0 Pa) across the specimens. The following are the main conclusions of this part:

1. The bare-surface permeable hollow-core block wall specimens exhibited a faster response during the first several hours of transient one-sided warming (in comparison to the more airtight surface-treated walls), even when no active pressure difference was induced across the wall, which may indicate a reduced dynamic attenuation of such walls. This aspect of hollow-core block wall performance deserves further investigation.
2. The Reynolds Number for the 1.25 m specimen height and a 0.15 m/s air velocity (rounded value for the measured 0.134 m/s) was ~12500, indicating that the cold room-side boundary layer flow may be laminar but not stable. The square root of Gr for the cold room-side surface of all the specimens was between 22900 to 27500

throughout the entire test period. The Richardson number under these circumstances was larger than 3, indicating that natural convection likely dominated in the cold room-side boundary layer. Based on these assumptions, the ranges of the estimated total surface heat transfer coefficient for all the four walls were within the bounds 6.59–7.69 W/m^2·K, which are 9% to 21% below the commonly used engineering value of 8.33 W/m^2·K.

3. The estimated steady-state R-values at the central and side cross sections of the regular-aggregate block were 0.50 to 0.65 m^2·K/W and 0.76 to 0.97 m^2·K/W for the lightweight aggregate block.
4. The small pressure difference increment across the wall specimens decreased the estimated areal heat flow rate from the specimen surface on the cold room-side by 1% to 3.5%, but did not affect the estimated apparent R-values. On the other hand, temperature difference between the warm box air temperature and the cold room air temperature were also reduced by 0.2°C ± 0.14°C for the HCRA and HCRA/BC specimens and by 0.1°C ± 0.14°C for the HCLA and HCLA/LCR specimens, with an identical effect on the difference between the box-side block surface temperature and the room air. This indicates that despite the reduced heat flow rate at the room-side surface, as claimed by researchers advocating dynamic insulation, more energy is needed inside the box to heat the incoming cold air. Consequently, it is suggested that whole envelope infiltration rates should be limited, say to a value of 0.1 ach at 50 Pa.
5. The bare block walls do not satisfy this criterion. The addition of an external cementitious brown coat or an internal lime cement rendering may supply this level of protection under natural infiltration, but not under whole dwelling underpressurization. It seems that the application of both layers should meet the requirement, but these tests have not been completed while producing this paper.

As a last remark, it is noted that the construction of the walls has been performed in the laboratory obeying stringent construction rules, with absolute care during the placement of joint mortar on the horizontal and vertical joints. Consequently, the results obtained in this investigation represent the lower limit of block wall infiltration rates. In-situ construction work usually involves many weaknesses that may accumulate some cracks and voids within the mortar, and especially to some separation between the blocks and structural elements (columns, beams, or floors), which, in turn, would probably lead to significantly increased infiltration rates. Further work should thus include laboratory studies simulating the effects of weak workmanship and wall joint deterioration, as well as field measurements of air tightness in existing buildings.

ACKNOWLEDGMENTS

The work presented in this paper was performed within the first stage of a research program on building envelope airtightness that is supported by the Israeli Ministry of Construction and Housing.

REFERENCES

ASTM. 2005. *ASTM C 1363-05, Standard Test Method for Thermal Performance of Building Materials and Envelope Assemblies by Means of a Hot Box Apparatus*. West Philadelphia, PA: American Society for Testing and Materials.

Dale, J.D., L.W. Kostiuk, and M. Hatzinikolas. 1985. Thermal performance of an insulated masonry structure in a northern climate. *Proceedings of the Third North American Masonry Conference., Arlington, Texas*, pp. 1–33.

Davies, M.G. 2004. *Building Heat Transfer*. West Sussex, England: John Wiley and Sons, Ltd.

Dumont, R.S., H.W. Orr, and D.A. Figley. 1981. Air tightness measurements of detached houses in the saskatoon area. Building Research Note 178, Division of Building Research, National Research Council, Canada.

Etheridge, D.W. 1977. Crack flow equations and scale effect. *Building and Environment* 12:181–89.

Feldman, D., C. Stathopoulos, H. Cosmulescu, and H. Wu. 1998. A simple apparatus for the evaluation of air infiltration through building envelope components. *Journal of Wind Engineering and Industrial Aerodynamics* 77&78:479–89.

Hagentoft, C.E. 2001. *Introduction to Building Physics*. Lund, Sweden: Studentlitteratur.

Hosni, M.H., J.M. Sipes, and M.H. Wallis.1999. Experimental results for diffusion and infiltration of moisture in concrete masonry walls exposed to hot and humid climates. *ASHRAE Transactions*105(2):191–203.

Khalifa, A-J.N. 2001. Natural convective heat transfer coefficient—A review I. Isolated vertical and horizontal surfaces. *Energy Conversion and Management* 42:491–504.

Kobus, C.J., and G.L. Wedekind. 1996. Modeling the local and average heat transfer coefficient for an isothermal vertical flat plate with assisting and opposing combined forced and natural convection. *International Journal of Heat and Mass Transfer* 39(13):2723–33.

Kostiuk, L.W., and J.D. Dale. 1987. Energy characteristics of a residential masonry structure. *ASHRAE Transactions* 93(1):482–96.

Kronvall, J. 1978. Testing of houses for air leakage using a pressure method. *ASHRAE Transactions* 84(1):72–79.

Mattsson, B. 2006. The influence of wind speed, terrain and ventilation system on the air change rate of a single-family house. *Energy* 31:719–31.

Nantka, M.B. 1986. Air infiltration and ventilation in relation to thermal performance of dwelling houses in Poland. *Building Services Engineering Research & Technology* 7(1):11–18.

Offermann, F.J. 1982. Residential air—Leakage and indoor air quality in Rochester, New York. Report 13100, Lawrence Berkeley Laboratory, Berkeley, CA.

Orme, M. 2001. Estimates of the energy impact of ventilation and associated financial expenditures. *Energy and Buildings* 33:199–205.

Poreh, M. 1992. Decreasing air infiltration in Israeli dwellings. Final Report, Technion Research and Development Foundation, Israel Institute of Technology, Haifa, Israel.

Poreh, M. 2004. Simple calibrator for low range differential pressure transducers. *J. Wind Engineering* 92:1167–70.

Probst, O. 2004. Cooling load of buildings and code compliance. *Applied Energy* 77:171–86.

SII. 1999. Determination of the characteristic thermal resistance of masonry walls. SI 1375, 1999, Standards Institution of Israel, Tel-Aviv, Israel. In Hebrew.

SII. 2000. General requirements and test methods for mortar for plaster. SI 1920 Part 1, 2000, Standards Institution of Israel, Tel-Aviv, Israel. In Hebrew.

SII. 2003. Thermal insulation of buildings: Residential buildings. SI 1045 Part 1, 2003, Standards Institution of Israel, Tel-Aviv, Israel. In Hebrew.

Sherman, M.H. 1980. Air infiltration in buildings. Report LBL 10712, Lawrence Berkeley Laboratory, Berkeley, CA.

Svec, O.J., and L.E. Goodrich. 1986. Natural convection in the cavity of a basement. *International Journal of Ambient Energy* 7(4):191–96.

Taylor, B.J., and M.S. Imbabi. 1997. The effect of air film themal resistance on the behavior of dynamic insulation. *Building and Envirnment* 32(5):397–404.

Yoshino, H., F. Haswgawa, and Y. Utsumi. 1984. Verification of calculation models of air infiltration using three types of test houses. *Proceedings of the 5th AIC Conference: The Implementation and Effectiveness of Air Infiltration Standards in Buildings, Reno, Nevada*.